AGU PUBLICATIONS

Tectonics

RESEARCH ARTICLE
10.1002/2016TC004269

Key Points:
- The 3-D structural map and geological cross section of the WAFTB east of Santiago
- Kinematics of deformation deduced from precise mapping of syntectonic Farellones formation
- Long-term shortening rate of 0.1–0.5 mm/yr, with possible deceleration by ~20 Ma

Supporting Information:
- Supporting Information S1
- Figure S1
- Data Set S1

Correspondence to:
M. Riesner,
riesner@ipgp.fr

Citation:
Riesner, M., R. Lacassin, M. Simoes, R. Armijo, R. Rauld, and G. Vargas (2017), Kinematics of the active West Andean fold-and-thrust belt (central Chile): Structure and long-term shortening rate, *Tectonics*, *36*, 287–303, doi:10.1002/2016TC004269.

Received 8 JUN 2016
Accepted 25 JAN 2017
Accepted article online 29 JAN 2017
Published online 22 FEB 2017

Kinematics of the active West Andean fold-and-thrust belt (central Chile): Structure and long-term shortening rate

M. Riesner[1], R. Lacassin[1], M. Simoes[1], R. Armijo[1], R. Rauld[1,2,3], and G. Vargas[2]

[1]Institut de Physique du Globe de Paris, Sorbonne Paris Cité, Université Paris Diderot, CNRS, Paris, France, [2]Departamento de Geofísica, Facultad de Ciencias Físicas y Matemáticas, Universidad de Chile, Santiago, Chile, [3]Now at Xterrae, Santiago, Chile

Abstract West verging thrusts, synthetic with the Nazca-South America subduction interface, have been recently discovered at the western front of the Andes. At ~33°30′S, the active San Ramón fault stands as the most frontal of these west verging structures and represents a major earthquake threat for Santiago, capital city of Chile. Here we elaborate a detailed 3-D structural map and a precise cross section of the West Andean fold-and-thrust belt based on field observations, satellite imagery, and previous structural data, together with digital topography. We then reconstruct the evolution of this frontal belt using a trishear kinematic approach. Our reconstruction implies westward propagation of deformation with a total shortening of 9–15 km accumulated over the last 25 Myr. An overall long-term shortening rate of 0.1–0.5 mm/yr is deduced. The maximum value of this shortening rate compares well with the rate that may be inferred from recent trench data across the San Ramón fault and the slip associated with the past two $M_w > 7$ earthquakes. This suggests that the San Ramón fault is most probably the only presently active fault of the West Andean fold-and-thrust-belt and that most—if not all—the deformation is to be released seismically.

1. Introduction

The central Andean mountain belt is viewed as the paradigmatic case example of a subduction orogeny [*Dewey and Bird*, 1970; *James*, 1971]. At latitude 33°S, east verging structures along the Argentinian eastern mountain front have for long been described (Figure 1) [e.g., *Ramos et al*., 1996, 2004; *Giambiagi et al*., 2001, 2003, 2011, 2014; *Farías et al*., 2010; *Garcia and Casa*, 2014; *Allmendinger and Judge*, 2014; *Fosdick et al*., 2015]. The less apparent evidence for active thrust tectonics on the western side of the Andes—directly facing the subduction zone—has so far been neglected (Figure 1). However, at ~33°30′S, Santiago, the capital city and largest conurbation of Chile, faces a >2 km high mountain front associated with the emergence of the San Ramón fault [*Armijo et al*., 2010] (Figure 2). Recent paleoseismological studies have shown that the San Ramón fault (hereafter SRF) hosted two paleo-earthquakes of M_w ~7.5 over the last 17–19 kyr [*Vargas et al*., 2014]. This emphasizes that the San Ramón fault is an active fault representing a significant seismic threat to the City of Santiago [*Armijo et al*., 2010; *Pérez et al*., 2013; *Vargas et al*., 2014]. *Armijo et al*. [2010] proposed a first-order model for the deeper structure of the San Ramón fault and found that it constitutes the frontal expression of a major west vergent fold-and-thrust belt that extends laterally for thousands of kilometers along the western flank of the Andes [see also *Armijo et al*., 2015]. However, an assessment of seismic hazard associated with this fold-and-thrust belt and specifically with the San Ramón fault needs improvement of our knowledge of their long-term characteristics: geometry, kinematics, and shortening rate.

We use earlier work by *Armijo et al*. [2010], who elaborated a map of the folded Cenozoic rocks that constitute the West Andean fold-and-thrust belt (hereafter WAFTB) and constructed a geological structural section of the western mountain front, providing first-order constraints on the timing of its tectonic deformation at the latitude of Santiago. Here by updating and refining that data set, we constrain more quantitatively (1) the geometry of the fold-and-thrust belt at depth, (2) the detailed kinematics of that belt, and (3) the shortening rates to be absorbed by folding and faulting. Then, we model the kinematic evolution of the WAFTB using a trishear approach [*Allmendinger*, 1998], and we derive precise constraints on incremental and cumulative shortening. Finally, we discuss the possible distribution of shortening and shortening rates accommodated over time across the overall WAFTB. These rates are compared with results obtained from paleoseismological trenches across the San Ramón fault [*Vargas et al*., 2014].

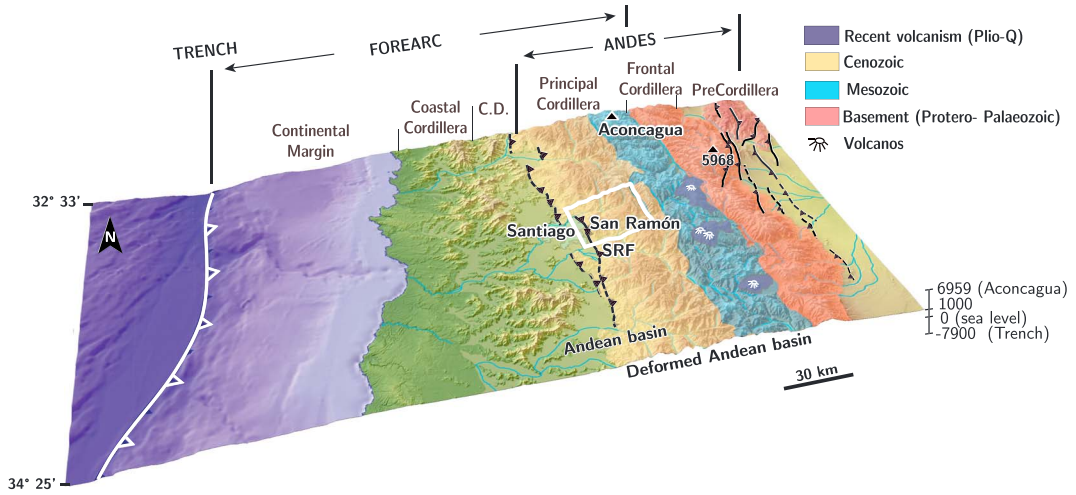

Figure 1. Physiographic view and first-order geology of the subduction margin of the Andes at ~33°S (central Chile and westernmost central Argentina). To the west, the trench marks Nazca-South America plate boundary (in white with open triangles). The Andes mountain belt, ~100 km wide at this latitude, is basically made of the Frontal Cordillera basement culmination to the east and of the folded and thrusted Mesozoic-Cenozoic rocks of the Principal Cordillera to the west. The San Ramón fault (SRF; black segmented line with triangles) marks the western Andean front facing the Central Depression (CD) and Santiago City. Main thrusts at the eastern Andean front are also indicated in black. See text for further description of geology and tectonic units. White rectangle locates our study area covered by the map of Figure 3.

2. Geological Setting

The central Andes mountain belt is related to the subduction of the Nazca Plate under the South American Plate and extends north-south over 4000 km from northern Peru to central-southern Chile. At the latitude of our study area (around 33°30′S), the plate boundary is characterized by four along-strike physiographic units (Figure 1): (1) the offshore continental margin including the subduction zone accretionary prism; (2) the onshore Coastal Cordillera constituted of Paleozoic and Mesozoic rocks and with elevations over 2000 m; (3) the Central Depression (CD) at an average elevation of ~500 m, filled with less than 1 km of Quaternary sediments; and (4) the Andes mountain belt with peaks commonly reaching elevations of 5000–6000 m and toping at ~7000 m at the Aconcagua. The City of Santiago is located within the Central Depression, just west of the morphologically well-defined West Andean Front that separates the depression from the Andes (Figure 2). The San Ramón fault at the base of this front was first described as a possible normal fault by *Tricart et al.* [1965] and *Borde* [1966] but has only been recently identified as an active thrust [*Armijo et al.*, 2010] with two M_w ~7.5 paleo-earthquakes over the last 17–19 kyr [*Vargas et al.*, 2014].

At the latitude of Santiago, the Andes mountain belt is composed of two principal structural units (Figure 1): (1) the Principal Cordillera to the west and (2) the Frontal Cordillera to the east. The Principal Cordillera consists of a folded and deformed 12–15 km thick sequence of Early Jurassic to Miocene volcanic and sedimentary rocks, deposited within the former—and now inverted—Andean basin [e.g., *Thiele*, 1980; *Mpodozis and Ramos*, 1989; *Vicente*, 2005; *Armijo et al.*, 2010]. The term Andean basin refers here to the units that have been deposited between the present-day Coastal and Frontal Cordilleras (Figure 1). The Principal Cordillera includes large tectonic units as the west vergent West Andean fold-and-thrust belt to the west [*Armijo et al.*, 2010] and the east vergent Aconcagua fold-and-thrust belt on its eastern side [*Ramos et al.*, 1996, 2004; *Giambiagi*, 2003; *Giambiagi et al.*, 2001, 2003]. The Frontal Cordillera consists of late Paleozoic units and pre-Andean Permo-Triassic volcanics [*Mpodozis and Ramos*, 1989; *Robinson et al.*, 2004; *Charrier et al.*, 2007]. In this study, we focus on the structure and kinematics of the West Andean fold-and-thrust belt (WAFTB; Figures 1 and 3).

The WAFTB affects the continental deposits from the Oligocene Abanico and Miocene Farellones formations [*Charrier et al.*, 2002, 2005] (Figure 3). The Abanico formation is composed of volcaniclastic rocks; tuffs; basic lavas; ignimbrites; and interbedded alluvial, fluvial, and lacustrine sediments [*Charrier et al.*, 2002, 2005; *Armijo et al.*, 2010]. It is at least 3 km thick, as can be observed on the western flank of the Cerro San Ramón (Figure 3). Ages ranging between 36 and 16 Ma have been proposed for the Abanico formation from a compilation of

Figure 2. The western front of the Andes above Santiago, capital city of Chile. (a) View to the southeast from Santiago downtown. The ~2.7 km high San Ramón mountain front is facing the Central Depression where Santiago city is located. The active San Ramón fault [*Armijo et al*., 2010] stands at the base of this mountain front. (b) Helicopter view of the San Ramón fault and large Santiago conurbation. San Ramón fault trace from *Armijo et al*. [2010]. Trench site where two M_w ~7.5 paleo-earthquakes have been identified, located north of Quebrada de Macul [*Vargas et al*., 2014]. East dipping Abanico beds are visible in right foreground (western flank of Cerro Abanico syncline).

ages at a regional scale [*Charrier et al*., 2002]. More precisely, at the latitude of our study area, K/Ar and $^{40}Ar/^{39}Ar$ ages on plagioclase in ash flows and lavas from this formation range from 30.9 to 20.3 Ma. The Abanico formation is also intruded by porphyric dikes as young as 16.7 Ma as derived from K/Ar age on whole rock [*Gana and Wall*, 1997; *Gana et al*., 1999; *Aguirre et al*., 2000; *Nyström et al*., 2003; *Vergara et al*., 2004]. The largest pluton intruding the formation close to Santiago is the La Obra leucogranodiorite, with $^{40}Ar/^{39}Ar$ biotite ages of 19.6 ± 0.5 Ma [*Kurtz et al*., 1997]. This suggests that the whole Abanico formation has been deposited prior to ~20 Ma. The Farellones formation is 1–2 km thick, composed of intermediate and basic lava flows and minor ignimbrite flows [*Beccar et al*., 1986; *Vergara et al*., 1988]. Age constraints for this formation, using K/Ar and $^{40}Ar/^{39}Ar$ on biotite and plagioclase, and U/Pb on zircons, in ash flows and lavas, range from ~21.6 to ~16.6 Ma east of Santiago [*Beccar et al*., 1986; *Nyström et al*., 2003; *Deckart et al*., 2005]. Both Abanico and Farellones formations are composed of volcaniclastic rocks and lavas, and the contact between these two units is described as progressive and unclear [*Charrier et al*., 2002, 2005]. However, the unconformity between the two formations (Figure 3) is identified at regional scale both in

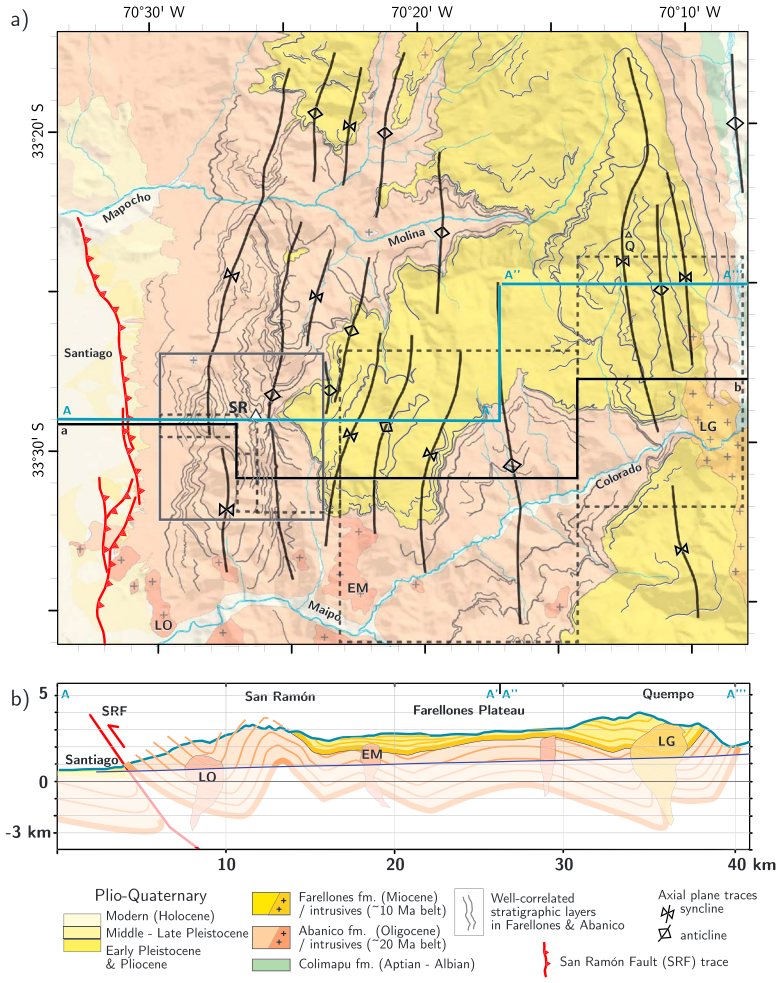

Figure 3. (a) Structural map of the West Andean fold-and-thrust belt (WAFTB), based on earlier map by *Armijo et al.* [2010] (see location in Figure 1), including well-correlated 3-D stratigraphic horizons (gray lines) mapped on DEM-based topography from observations on satellite imagery and aerial photographs, checked carefully with systematic field observations. Here the traces of the 3-D layers are significantly refined by using high-resolution satellite images from the Google Earth database (Landsat 7, DigitalGlobe), digital elevation models (ASTER DEM ~30 m resolution), and new helicopter views (Figures 4 and 5). For simplicity, we only represent here horizons that correlate well over several kilometers in Abanico and Farellones formations. Additional details are provided as supporting information, in particular finer stratigraphic horizons required for the projection on the cross section (see Figures S1 and S2). Major anticline and syncline axes are represented by black arrowed lines. SRF: San Ramón fault, Q: Cerro Quempo, LO: La Obra pluton, EM: El Manzano pluton, LG: La Gloria pluton. Dashed-line rectangles correspond to the swaths used for the projection of horizons along the a-b section (in black; see text and Figures 4 and S1 for further explanations). AA′-A″A‴ section (in blue) represents here the topographic profile, with the minimum altitude required for projecting all structures observed within the swath boxes. Box in black locates Figure 4a. Strike and dip measurements are extracted from 3-D mapped continuous horizons, not from discrete field measurements of small-scale features (see text for further explanations). Georeferenced horizons can be retrieved from the supporting information. (b) Synthetic subsurface cross section representing form lines deduced by projecting stratigraphic horizon geometries with the swath boxes along section a-b, with the maximum elevation along the combined sections A-A′ and A″-A‴ (Figure 3a; see Figure S2 in the supporting information for the detailed stratigraphic horizon projection). Figure 4 further illustrates our projection technique. Direct surface observations are possible from mountaintops down to valley bottoms. Interpretation at depth is deduced from this subsurface projection and represented with transparency. Thin blue line reports Maipo and Colorado River bed profiles that define the limit between directly observed structures and extrapolations at depth.

the field and on aerial and satellite imagery [*Armijo et al.*, 2010]: the Abanico formation appears to be more strongly folded than the overlying Farellones formation.

The Oligo-Miocene Abanico and Farellones formations were deposited above Mesozoic sedimentary series that now outcrop as a ~9 km wide nearly vertical limb of a large west verging fold exposing these

Mesozoic rocks east of our study area [*Thiele*, 1980; *Armijo et al*., 2010]. Two main formations can be identified. The Lo Valdés formation is a Late Jurassic-Early Cretaceous calcareous series. Outcropping east of this series, the Late Jurassic Río Damas formation is composed of ~3 km thick continental conglomerates, andesitic lavas, and breccias. A regionally well-known gypsum layer of Late Jurassic age (Yeso Principal del Malm [*Thiele*, 1980]) has been observed nearby the base of the Oligo-Miocene and Cretaceous series of this Andean basin sedimentary pile. The basal detachment of the West Andean fold-and-thrust belt is likely localized within this Late Jurassic gypsum layer [*Armijo et al*., 2010].

Armijo et al. [2010] conducted a structural investigation and proposed a geological map of the WAFTB constrained by stratigraphic horizons mapped in 3-D, with a particular emphasis on the definition and mapping of the stratigraphic limit between Farellones and Abanico formations over all our study area. By projecting stratigraphic horizons, *Armijo et al*. [2010] proposed a first-order cross section of the WAFTB. Folding of the Abanico and Farellones formations is interpreted as resulting from a succession of west vergent faults that root into a décollement at depth. Only the most frontal fault, the San Ramón fault, reaches the surface (Figure 2). Those results suggest that the whole Abanico formation has undergone a similar amount of folding, whereas deformation decreases rapidly upward into the Farellones formation [*Charrier et al*., 2002; *Armijo et al*., 2010]. However, the level of accuracy in the 3-D mapping of stratigraphic horizons in the Abanico and Farellones formations and on the contact between the two formations is not sufficient to conduct a detailed study of the WAFTB kinematics.

3. Geometry of the West Andean Fold-and-Thrust Belt

3.1. Building a Self-Consistent Geological Map of the West Andean Fold-and-Thrust Belt

Because of their initial depositional—volcanic and clastic—continental environments, the geometry of Abanico and Farellones layers may show important local-scale geometric variations not related to tectonic deformation. In addition, later dike intrusions—originally vertical or oblique to layering—disrupt very often that geometry. These characteristics have for long inhibited precise structural studies of the western Andean front. However, at a larger observational scale, such as from satellite images, the overall structural geometries are clearly visible (Figures 3 and 4). For these reasons, structural mapping by *Armijo et al*. [2010], *Rauld* [2011], and in this study has essentially relied on large-scale observations of structures clearly identified on high-resolution satellite and aerial imagery, complemented and systematically checked by field observations of those structures, which are typically well identified at the scale of the landscape (from 1 m to 100 m and more). Indeed, we deliberately discarded to rely on standard approaches using statistical analyses of numerous outcrop-scale ($\lesssim$~10 m) strike-and-dip measurements, which clearly contain—in most of the WAFTB—much noise associated with depositional volcanic environments. One particularly well-constrained example of our cartographic approach is the continuous trace of the contact separating Farellones formation from Abanico formation, which is readily identified over tens of kilometers in the landscape, both in the imagery and in the field. Less continuous bedding surfaces represented in our maps and sections are fundamental elements characterizing the structural fabric of strain and its variations in 3-D mainly within the Abanico formation (see Figures 4 and S1 and S2 in the supporting information).

The detailed structural map of the WAFTB presented here is based on *Armijo et al*. [2010]. It integrates stratigraphic layers in 3-D, which are now significantly refined by using (1) high-resolution satellite images from the Google Earth database (Landsat 7, DigitalGlobe) and aerial photographs, together with (2) digital elevation models (Advanced Spaceborne Thermal Emission and Reflection Radiometer DEM ~30 m resolution; Figures 3 and 4). Our refined, high-resolution, and large-scale structural map and subsurface cross section as well as our georeferenced 3-D stratigraphic horizons are provided in Figures S1 and S2 and Data Set S1 in the supporting information. Such high resolution is crucial to precisely derive the folding geometry of the Abanico and Farellones formations and therefore to constrain the kinematics of folding and thrusting of the belt.

3.2. Building a Geological Cross Section of the West Andean Fold-and-Thrust Belt

To build our detailed cross section (Figure 3), we projected the 3-D georeferenced stratigraphic layers within swath boxes on an east-west section labeled a-b in Figure 3a. The east-west A-A‴ section (combined sections A-A′ and A″-A‴ to better represent the folded structures just to the north of Río Colorado—Figures 3 and 4 and high-resolution section in Figure S2) corresponds to the topographic profile with the maximum

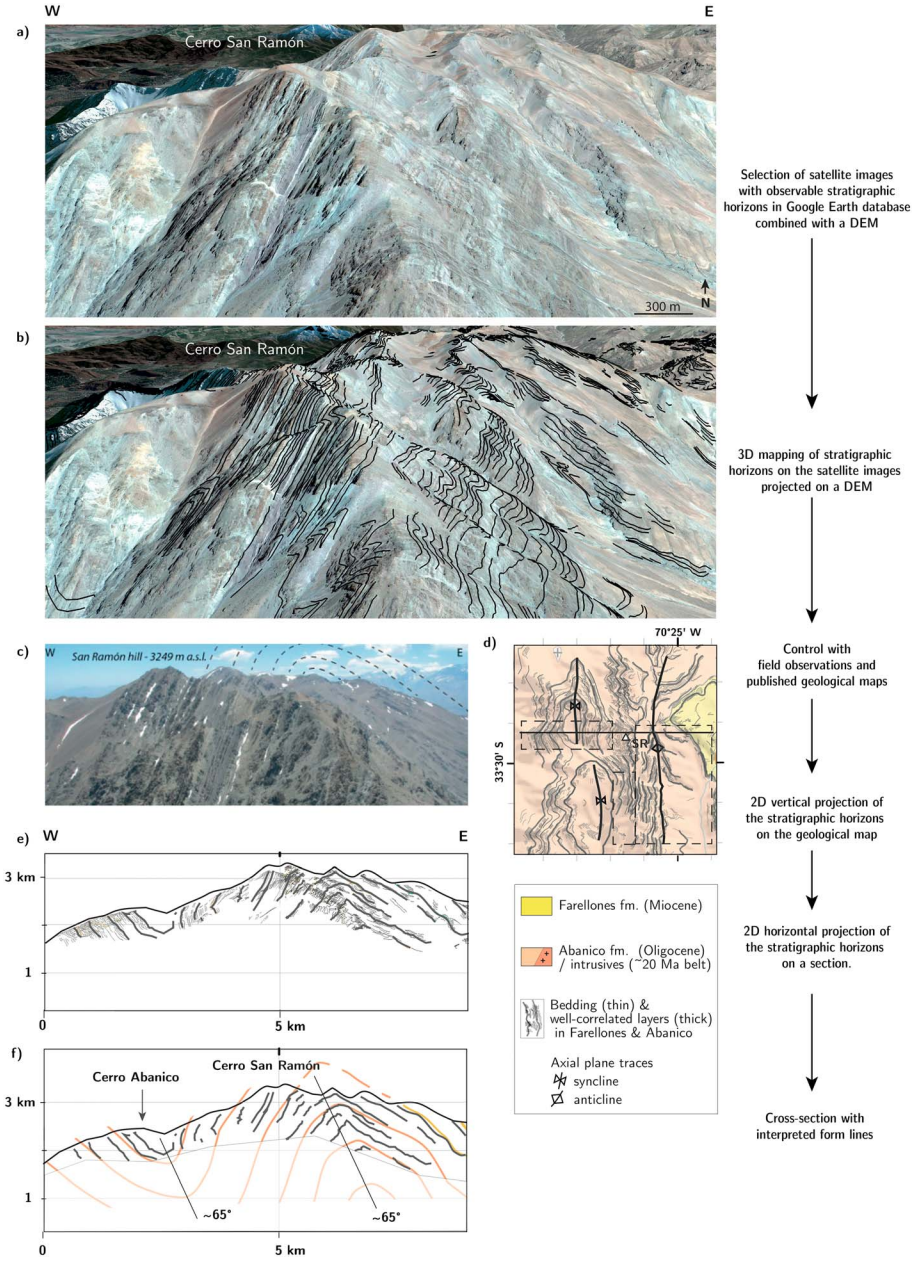

Figure 4. Construction of our 3-D map, illustrated from the specific example of the Cerro San Ramón. (a) High-resolution satellite image of the Cerro San Ramón from the Google Earth database (Landsat 7, DigitalGlobe) projected on a digital elevation model. (b) Same satellite image with the visible stratigraphic horizons mapped in 3-D. (c) Field picture of the Cerro San Ramón. (d) Structural map of Cerro San Ramón (SR; black box in Figure 3a). The 3-D stratigraphic horizons within the swaths marked by dashed boxes are projected onto the section. No strike and dips are represented on the map as we mapped continuous horizons in 3-D (see text sections 3.1 and 3.2 for further explanations). Discontinuous stratigraphic horizons are in gray and well-correlated ones are in black. (e) E-W section showing bedding altitudes, obtained by projecting the structural elements (stratigraphic horizons) mapped on the DEM within the dashed boxes (Figure 4a). Discontinuous stratigraphic horizons are in gray and well-correlated ones are in black. (f) Synthetic cross section deduced from Figure 4b, showing geometry of the Cerro San Ramón folded structure. The San Ramón anticline and associated Cerro Abanico syncline appear reversed with a clear west vergence. See Figures 5a and 5b for the aerial views of these folds. Well-correlated stratigraphic horizons are in black, and interpreted form lines are in orange (Abanico formation) and in yellow (Farellones formation). Gray lines represent the elevation envelope within the swath profiles.

altitude (passing by San Ramón and Quempo summits), required to project all structures observed within the swath boxes. River incision, in particular along the Río Colorado, offers very favorable conditions for direct subsurface observations of bedding geometry. Stratigraphic horizons, mapped in swath boxes and along a-b, can readily be projected along A-A‴ from our map, allowing us for deriving a precise subsurface cross section over a depth of ~4 km (Figure 3). The projection technique, illustrated by the example of the San Ramón fold shown in Figure 4, is as follows: (1) the elevations along each mapped individual well-defined bedding traces are measured from the DEM; (2) these 3-D stratigraphic horizons are projected onto a west-east direction (perpendicular to the average trend of fold axes across selected 2 to 17 km wide swaths, indicated by boxes shown by dashed lines in Figures 3 and 4), with swath widths chosen to avoid noncylindrical complexities; (3) this results in an E-W structural section displaying all stratigraphic horizons across the width of the swaths (see Figure 4e); and (4) then, from this factual structural section an interpretative geometry is deduced with form lines averaging the overall geometry of projected stratigraphic horizons (Figure 4f).

Our approach enabled us to build a precise subsurface structural section including variation in bedding attitude over a wide range of elevation (4 km; see Figures 3 and S2), despite local uncertainties related to the difficulty of following discontinuous volcanic layers or to the presence of intruding plutonic complexes. This section clearly illustrates in detail all major structural features of the fold-and-thrust belt: the frontal San Ramón fold (Figure 4), the geometry of the layers within the Farellones formation overlying the succession of folds within the central part of our study area, and the subvertical Abanico and Farellones layers to the east.

From the foregoing detailed section, we build a general cross section illustrating the structures of the WAFTB across our study area (Figure 6), by extrapolating at depth our above-mentioned subsurface observations. The undeformed footwall of the San Ramón fault and WAFTB is proposed to be composed of slightly east dipping Mesozoic and Cenozoic layers, as can be deduced from regional geological maps [*Thiele*, 1980; *Gana et al*., 1999; *Sellés and Gana*, 2001; *Fock*, 2005] and the known stratigraphy of the Andean basin [*Charrier et al*., 2002; *Charrier et al*., 2005; *Robinson et al*., 2004; *Armijo et al*., 2010]. We combine these data with geological observations on the thickness of the Abanico/Farellones formations and on the Mesozoic series outcropping slightly further east from our study area, within an almost vertically dipping west vergent fold limb [*Thiele*, 1980; *Armijo et al*., 2010]. From there we derive the total thickness of the Andean basin series to ~12–15 km. Following *Armijo et al*. [2010], we propose that the anticlines grow above underlying faults that root at depth into a regional décollement. Given the general thickness on the folded Meso-Cenozoic series and the probable mechanical contrast between basement and sediments, we propose that the décollement lies at the base of the Andean basin series, within a possible 10–15 km deep level of Jurassic gypsum observable in the folded Mesozoic series of the Principal Cordillera [*Thiele*, 1980; *Armijo et al*., 2010] (Figure 6).

3.3. Geometry and Kinematics of Deformation of the West Andean Fold-and-Thrust Belt, as Constrained From Map and Field Observations

Figure 6 summarizes our structural interpretation of the WAFTB. It is to the first-order comparable to that of *Armijo et al*. [2010], however with more precise constraints on the subsurface geometries of folds and in particular of the angular unconformity between Farellones and Abanico formations, as needed for a detailed kinematic reconstruction of the evolution of this fold-and-thrust belt. The WAFTB is characterized by five anticlines with westward decreasing wavelengths from ~13 to ~5 km. The folds are overturned with their western flanks overall steeper than their eastern ones (Figures 3–6), clearly indicative of a westward structural vergence. At depth, this succession of folds is interpreted as involving five steeply dipping faults rooting onto a basal décollement within possible Jurassic gypsum. These faults are hereafter labeled F0 to F4, from east to west, F4 corresponding to the frontal San Ramón fault (Figure 6). The westward decreasing wavelengths of anticlines is reflected at depth by more closely spaced faults toward the west. All faults—except the most frontal San Ramón fault (Figure 2)—do not reach the surface, so that anticlines are interpreted as fault-propagation folds. Along the western front of the WAFTB, the San Ramón fault reaches the surface with a cumulative stratigraphic throw of ~4–5 km (Figure 6). There are large uncertainties on the shortening accommodated by F0 due to the presence of the large La Gloria pluton intruding the layers deformed by this fault. We restored our cross section and estimated the total shortening to be of 9–15 km on F1 to F4 either from a line length or area balance approach, consistent with the rough estimate of *Armijo et al*. [2010]. This value does not include additional 1 to 5 km of shortening on F0.

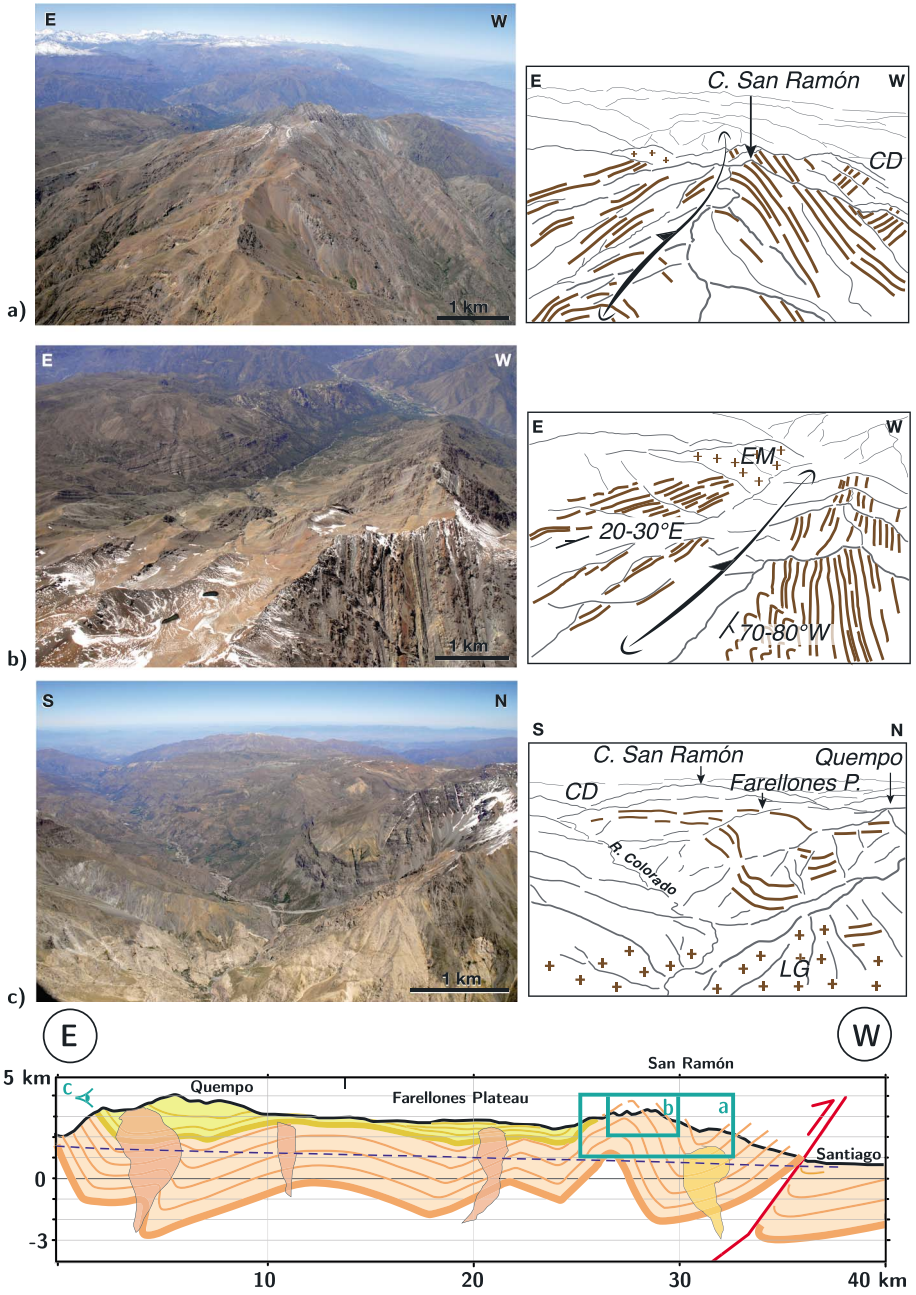

Figure 5. Low-altitude helicopter views of the West Andean fold-and-thrust belt (WAFTB) and corresponding interpretative sketches (to the right). These observations are located with respect to our subsurface cross section (bottom), here displayed mirrored with respect to Figure 3 to allow for an easier comparison between structure and field photographs. (a) San Ramón folded structure at the western front of the WAFTB just east of Santiago City (view to the south). The large reversed San Ramón anticline (fold axis shown on interpretative sketch) and the associated Cerro Abanico syncline to the west are facing the Central Depression (CD). (b) View to the south from above San Ramón summit showing in details the structure of the San Ramón anticline. The anticline is asymmetric with beds dipping 70–80°W on average on its western flank, while dip angles of 20–30°E characterize its eastern flank. The anticline axis is indicated on the interpretative sketch to the right. In the background, the El Manzano pluton (EM) is visible, as well as part of the Río Maipo valley. (c) Panorama of the WAFTB, view to the west from above the Colorado valley south of the Cerro Quempo crest (location of viewpoint on section). The large Quempo reversed syncline and the broad westward anticline topped by the Farellones Plateau are visible in the middle of the photograph. The San Ramón crest spreads N-S in the background. In the foreground, the La Gloria (LG) pluton intrudes folded structures of the eastern side of the WAFTB.

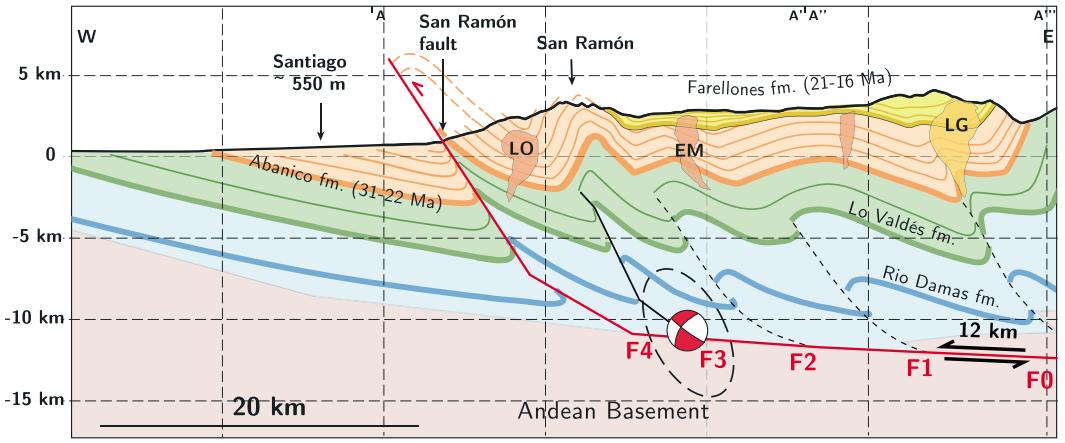

Figure 6. Interpreted deep geometry of the West Andean fold-and-thrust belt. Structures above ~4–5 km depth are directly deduced from geological observations (Figures 3 and 5), while deeper structures are extrapolated. The fold-and-thrust belt is characterized by five anticlines associated with blind fault ramps (F0 to F3) and, to the west, by the San Ramón fault (SRF; labeled here F4) that reaches the surface along the western topographic front. At depth, the faults root onto a décollement located in Jurassic series at the base of the Mezosoic Andean basin. Miocene plutons are represented in orange: La Obra (LO; ~20 Ma [*Kurtz et al*., 1997]), El Manzano (EM), and La Gloria (LG; ~10 Ma [*Cornejo and Mahood*, 1997; *Deckart et al*., 2010]). The focal mechanism represented is an average focal mechanism calculated by *Pérez et al.* [2013] for 11 earthquakes with well-constrained locations and depths in this area. The dashed ellipsis represents the uncertainties in average hypocentral location.

In agreement with *Charrier et al*. [2002] and *Armijo et al*. [2010], we observe a progressive contact between the Abanico and Farellones formations. The Abanico formation is overall conformably folded. However, this is not the case for the Farellones formation: within this series, deformation gradually decreases upward and some angular unconformities are observed between the two formations (Figures 3 and 6). These observations imply that deformation of the WAFTB started after deposition of the Abanico formation—i.e., after 25–22 Ma—but overall before deposition of the Farellones formation by ~22 Ma [*Charrier et al*., 2002; *Armijo et al*., 2010]. However, some additional constraints on the timing of deformation of the different faults F0 to F4 affecting the WAFTB can be gained from our 3-D mapping of layers. In the case of F0, no clear observations on the geometry of the Abanico or Farellones layers are available as most of the record is obscured by the La Gloria pluton along the Río Colorado (Figures 3 and 6). The Farellones formation seems to be slightly folded, but our observations are insufficient to clearly document whether there could be an unconformity between Abanico and Farellones. From this, we cannot determine if deformation on F0 started before or after deposition of Farellones formation. Westward, the Farellones formation lies unconformably over the Abanico formation over the two anticlines associated with F1 and F2. Here the base of the Farellones formation is slightly folded, but the uppermost layers are not folded, with some onlap features on the western flank of the anticline associated to F1. We therefore infer that deformation on F1 and F2 initiated after deposition of the Abanico formation and before that of the Farellones formation and that it stopped during the early deposition of the Farellones formation. In the case of F3, all the Farellones layers—still preserved on the eastern flank of the associated anticline—are conformable to the Abanico formation, with no particular evidence of an angular unconformity. The uppermost Farellones layers are however absent here, either because they have been eroded or never deposited on the eastern flank of this anticline. From this, we infer that deformation on F3 started well after the beginning of deposition of the Farellones formation and even perhaps after the end of its deposition. As of F4 (San Ramón fault), we do not have any particular constraints on its timing due to the lack of evidence from growth layers or unconformities between Farellones and Abanico formations. Therefore, our detailed 3-D mapping (Figures 3 and 6) is consistent with an overall—and classical—westward propagation of deformation on the faults within the WAFTB, with some precise constraints on the timing of faults relative to the deposition of the Farellones formation (Figure 7). To this respect and given the evidence of present-day active faulting [*Armijo et al*., 2010; *Vargas et al*., 2014], we hypothesize that the frontal San Ramón fault (F4) is the most recent of these faults.

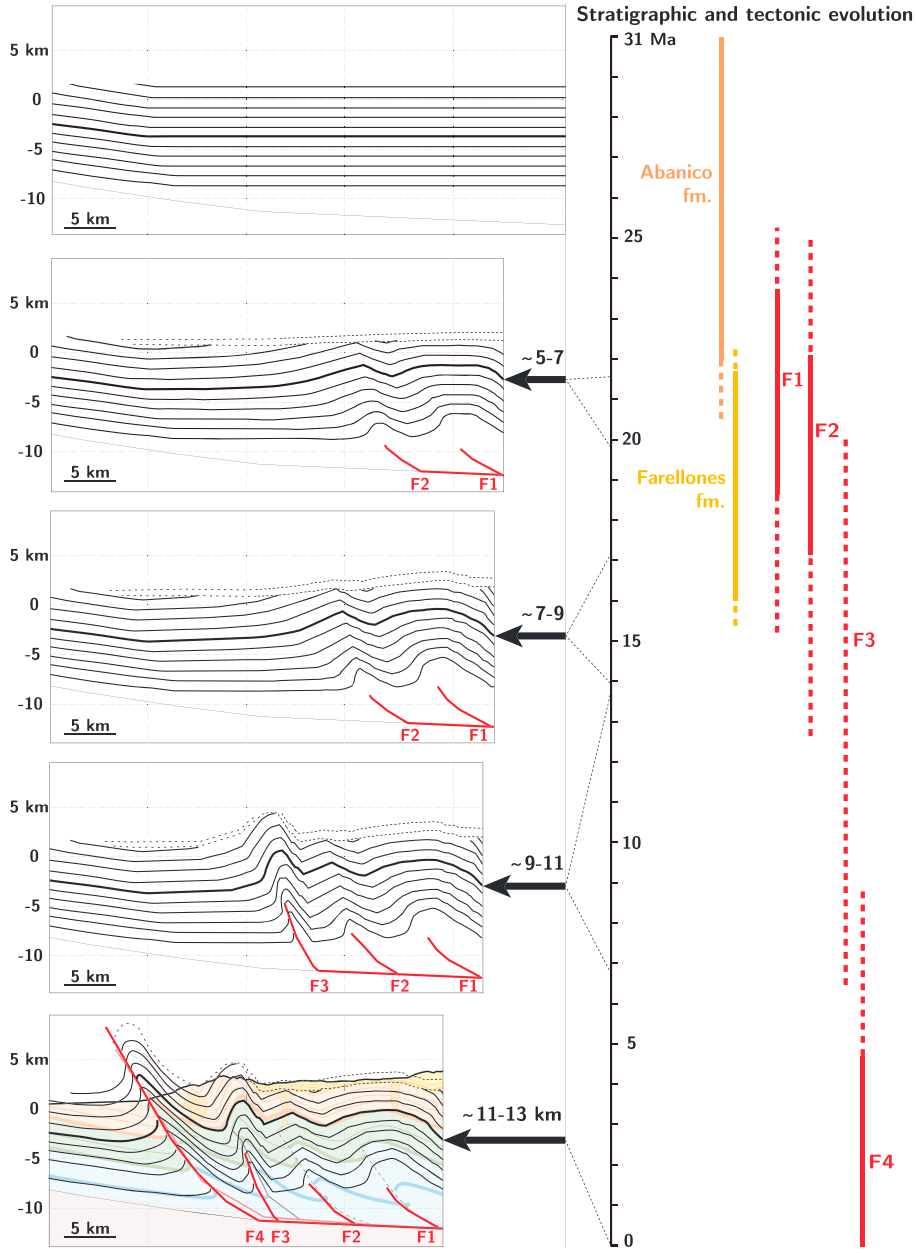

Figure 7. (left) Kinematic evolution of the West Andean fold-and-thrust belt from trishear modeling performed with FaultFold Forward version 6 (freely available from http://www.geo.cornell.edu/geology/faculty/RWA/programs/faultfold-forward.html [*Allmendinger*, 1998]). The folded structure is modeled by four propagating on-sequence faults ramping up from a décollement. The faults are labeled F1 to F4, with reference to the section of Figure 6. Only the most frontal fault, F4, corresponding to the active San Ramón fault propagates to the surface. Dashed lines indicate the layers added at the surface during modeling to simulate deposition of the syntectonic Farellones formation. (right) Synthesis of chronological constraints, as deduced from growth strata within the Farellones formation (see text for further discussion).

4. Modeling the Kinematics of Deformation of the West Andean Fold-and-Thrust Belt

The geological inferences on the style of deformation, shortening, and timing of deformation are further explored in a forward kinematic model of the WAFTB (Figure 7). We use here the formalism for trishear folding [*Erslev*, 1991] as folding is in our case interpreted mostly as fault-propagation folding. We use the code FaultFold Forward version 6 freely available from http://www.geo.cornell.edu/geology/faculty/RWA/programs/faultfoldforward.html [*Allmendinger*, 1998]. Trishear modeling of folding simulates triangular zones of distributed deformation at the tip of propagating faults. In our model approach, folding is calibrated by

seven parameters: the propagating fault ramp angle, the coordinates of the propagating fault tip, the slip on the fault, the trishear angle (i.e., the angle of the triangular zone with distributed deformation at the tip of the fault), the inclined shear angle controlling the backlimb kinematics (either parallel or similar folding), and the fault propagation (*P*) to fault slip (*S*) ratio (*P*/*S*). Our geological cross section provides inferences on the general final fold geometry, on the fault ramp angles, propagating fault tip, and on the final stratigraphic throw across the faults. The ratio *P*/*S* cannot be constrained from direct geological observations [*Allmendinger and Shaw*, 2000]. Its influence on the fold shape has been described by numerous authors [e.g., *Hardy and Ford*, 1997; *Allmendinger*, 1998; *Zehnder and Allmendinger*, 2000; *Allmendinger and Shaw*, 2000]. Based on these studies and using our geological constraints, we defined by trial and error a set of parameters (Table S1 in the supporting information) that best satisfactorily reproduces the geometry of the folds and proposed kinematics of the WAFTB (Figure 7). We acknowledge that this set of parameters may not be unique. In any case, our main inferences (see discussion below) most exclusively depend on the progressive accumulation of shortening and on the timing of deformation that directly derive from geological observations. Modeling is here essentially used as an illustration and as a viability test for the inferred kinematics.

We assume that layers were initially horizontal within the deformed part of the Andean basin to the east, with layers slightly east dipping on the undeformed western side. Syntectonic deposition is modeled by adding additional sedimentary layers during ongoing deformation, so as to reproduce the angular unconformity observed between Farellones and Abanico formations. Modeled faults ramp-up from a regional décollement with an eastward dipping angle of 4°. In particular, we model the initiation, propagation, slip and—whenever applicable—the termination of activity of faults F1 to F4. The timing of fault activity follows geological observations as described above and is given with respect to deposition of the Abanico and above all Farellones formations (Figure 7). Cumulative shortening is constrained from our geological cross section to 9–15 km on F1 to F4 (Figure 6). We do not attempt to model F0, as too few observations on the subsurface geometry of folded layers (either Abanico or Farellones) are available along our cross section.

Our best fitting model that accounts for the overall geometry of folds and for the timing of deformation is represented in Figure 7. From this model, we can easily interpret the geological cross section in terms of cumulative shortening over time. Indeed, we find a cumulative shortening ranging from 6 to 7 km on F1 and F2 prior to deposition of the Farellones formation, increasing to 7–9 km after the deposition of the Farellones formation stopped. After that, cumulative shortening gets to 9–11 km with slip on F3. Initiation and activity of F4 (San Ramón fault, still active today) add additional deformation and reach a final cumulative shortening of 11–13 km, in agreement with the range of total shortening estimated from our geological cross section. The modeled final geometry fits reasonably well our geological cross section (Figure 7, final sketch), in particular at the subsurface where detailed geological observations are available. We therefore do find that our geological cross section and our several inferences on the kinematics and timing of deformation can be reasonably well reproduced from a system of faults propagating westward, i.e., toward the front of the WAFTB and the Central Depression (Figure 1).

Finally, we use our reconstruction of the kinematics of the WAFTB to quantify the evolution of cumulative shortening relative in time to the present-day situation, i.e., as if unfolding backward in time our cross section. The results are represented in Figure 8. Uncertainties on shortening and on the timing are large (of the order of ~5 km for shortening and of 4–9 Ma for timing) but still allow for illustrating the general kinematics of the WAFTB. Indeed, we do find that our incremental reconstruction of the WAFTB can be reasonably well reproduced by considering a shortening rate of 0.3 to 0.5 mm/yr over the last ~25 Myr, consistent with the estimate of *Armijo et al*. [2010] (Figure 8).

5. Discussion

5.1. Uncertainties on Our Geological Cross Section and Kinematic Modeling

5.1.1. Uncertainties on Our 3-D Map and Geological Cross Section

Our geological and structural map is based on a novel approach by considering stratigraphic layers in 3-D. Because we do not build our section only from local observations (as can be classically done along major river incisions) but by integrating the local geometrical variability of layers in 3-D along ~2 to 17 km wide swaths (Figures 3–5), we estimate our subsurface observations (down to 3–4 km depth) to be representative of the investigated structures over our study area. However, our results and observations depend on the

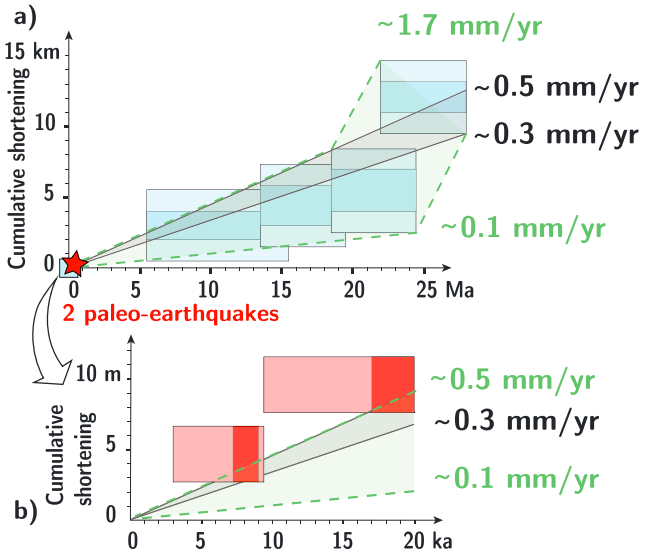

Figure 8. Evolution of tectonic shortening across the western Andean fold-and-thrust belt (WAFTB) since ~25 Ma. (a) Cumulative shortening (relative to present day) across the WAFTB as a function of time, as deduced from our geological observations (Figures 3–6) and kinematic model (Figure 7). The four blue boxes represent the shortening accumulated during the four time intervals separating the five temporal steps shown in Figure 7. The dimensions of the boxes represent the range of possible values for shortening (as deduced from our modeling) and timing. An additional 2–3 km uncertainty is represented in light blue and corresponds to the uncertainty estimated from our hand-drawn cross section. These data are consistent with a long-term average shortening rate of 0.3–0.5 mm/yr over the last 25 Myr. The data may however suggest more complex kinematics with an initial higher shortening rate of ~1.7 mm/yr prior to ~18–22 Ma, followed by a lower rate of 0.1 to 0.5 mm/yr from ~20 Ma to present day (see discussion in text).(b) Comparison between long-term shortening rates deduced from Figure 8a and occurrences of the two paleo-earthquakes documented by trenching across the San Ramón fault (red boxes [*Vargas et al.*, 2014]). Larger, light red boxes represent the additional uncertainties in time based on the available age constraints [*Vargas et al.*, 2014].

continuity and reliability of the observed layers. In particular, as discussed earlier in this paper, because the Abanico and Farellones formations are essentially of volcanic and volcano-detrital origins, their layers can be discontinuous in space and time. Large plutons, intruding the Abanico and Farellones formations, exist in our study area and in some cases obscure locally the geometry of layers. At the level of the Cerro Quempo, along the Río Colorado and to the east of our study area, the large La Gloria pluton impedes clear observations of the deformed layers of the Abanico and basal Farellones (Figures 3 and 6). Overall, we believe that such uncertainties, either related to discontinuous volcanic layers or to intrusions, were mostly unraveled by integrating stratigraphic horizons in 3-D in ~2 to 17 km wide swaths, i.e., over a large volume of rock (of the order of 10^3 km^3). We estimate that the remaining uncertainty related to our mapping and hand-drawn structural reconstruction would contribute to an ~2–3 km variability on our total shortening estimate, with an additional uncertainty of ~2–3 km when integrating the anticline beneath the Cerro Quempo.

Our subsurface observations (Figures 3–5) were then extrapolated at depth to build the composite cross-section A-A‴ (Figure 6). One of the uncertainties at depth is the location of the décollement. East of our section, deformed Mesozoic series crop out, implying that the WAFTB basal décollement is located under these series [*Armijo et al.*, 2010]. The thickness of the Lo Valdés and Río Damas formations at this latitude is ~9 km. Based on field observations, we estimated a thickness of ~3–4 km for the Abanico formation at the Cerro San Ramón and around 2–3 km under the Cerro Quempo, where it appears to have been more strongly eroded before Farellones deposition. The Farellones formation reaches a thickness of ~2–3 km at the Cerro Quempo. The overall thickness of the deformed Andean basin at this location seems to be 12–15 km with a décollement therefore located at a depth of 11 to 13 km. We chose an average dip of 4° for the décollement following *Armijo et al.* [2010]. Our field observations and interpretations are different than those proposed by *Ramos et al.* [2004]. They propose a thinner thickness for the Andean basin and a basal décollement depth also at 12–15 km, however, located in the pre-Andean basement.

The dip of the faults is constrained from the fold geometries at the subsurface. For comparison, we show in Figure 6 the average focal mechanism calculated by *Pérez et al.* [2013] for 11 earthquakes with well-constrained locations and depths in this area. Please note that this focal mechanism is not that of a particular seismic event but is rather an average of several earthquakes, all located within an area extending over a 5 km distance and 6–13 km depth range. The depths of these events, as well as the strike and dip of the east dipping nodal plane, appear fully compatible with the proposed West Andean structure.

5.1.2. Uncertainties on Our Chronological Constraints

Our kinematic reconstruction is essentially given relative to the Farellones formation, based on the presence or absence of angular unconformities between this formation and the Abanico formation, above growing anticlines and associated propagating faults. Here we define the base of the Farellones formation by mapping the angular unconformity between Abanico and Farellones formations. The geometrical contact is easier to follow at a regional scale than a limit based on local stratigraphy only and allows us for better constraining the unclear limit between the two formations.

Our chronological constraints depend on the absolute dating of the base of the Farellones formation. As mentioned before, age constraints for the Farellones formation, using K/Ar, $^{40}Ar/^{39}Ar$ on biotite and plagioclase, and U/Pb on zircons, range from ~21.6 to ~16.6 Ma east of Santiago [*Beccar et al*., 1986; *Nyström et al*., 2003; *Deckart et al*., 2005]. More precisely, there is no exact constraint on the absolute age of the upper member of the Abanico formation and of the lower member of the Farellones formation. The youngest age found for the upper part of the Abanico formation lower member is 25.2 (±0.1) Ma from K-Ar dating on plagioclase in ash flows and lavas [*Vergara and Drake*, 1979], and the lower part of the middle member of the Farellones formation is 21.6 (±0.2) Ma using $^{40}Ar/^{39}Ar$ on plagioclase in lavas [*Aguirre et al*., 2000]. The base of the Farellones formation is located ~700 m under the sample dated to 21.6 (±0.2) Ma and ~1200 m above the one at 25.2 (±0.1) Ma. This implies an age between 21.6 (±0.2) and 25.2 (±0.1) Ma for the base of the Farellones formation, probably closer to ~22–23 Ma. Therefore, within our kinematic reconstruction, we consider an uncertain range between 21.6 and 25.2 Ma for the base of Farellones formation and the top of Abanico formation.

5.1.3. Uncertainties Related to Our Forward Kinematic Modeling

Figure 7 illustrates our preferred forward kinematic model, obtained using the parameters summarized in Table S1. The best fitting parameters were approximated by trial and error in ~50 model tests, so as to fit the observed geometry of deformed layers. The observed subsurface geometry provides information on five of the seven parameters. The *Y* coordinate of the initiation of the fault is chosen on the décollement dipping at 4° to the east as detailed above. The *X* coordinate is determined by the final horizontal location of the fold at the surface. It is well constrained by trial and errors in our model with a variability of up to 3 km depending on the choice of other parameters. The three other parameters, also derived from the subsurface geometry of the layers and the shortening accumulated on each fold, are the slip on the fault, the ramp angle, and the inclined shear angle. The uncertainty in cumulative shortening and fault slip, step by step, in Figure 7 is derived by trial and error and represents the range of possible values. That range of values is dependent on the choice of parameters for each individual step and well as on the choice of parameters for all previous steps in our modeling procedure. Overall, we find that fault slip is constrained in our model with a maximum uncertainty of 1500 m for F1. The faults initiate with a small ramp dip and, as the faults propagate, they steepen. The dip of the fault ramps is well constrained by the subsurface fold geometries with a 4° variability on the dip angle but with larger uncertainties at depth (dip angle variability at depth of 10°). From there we propose that the faults F1 and F2 dip at 38–49°, whereas F3 and F4 are steeper, dipping, respectively, at 50–60° and 45–55°. The inclined shear angle controls the shape of the fold backlimb [*Cristallini and Allmendinger*, 2002]. In the model, the geometry of the backlimb is controlled by asymmetric similar folding with shear-inclined angles between 18° and 20° and between −20° and −18° (angles measured relative to the vertical). The two remaining parameters are the trishear angle and the *P*/*S* ratio. The trishear angle controls the size of the deformed area. In a trishear zone with small apical angles, intense strain is concentrated in a narrow wedge of rocks. If the apical angle progressively reduces during fault propagation, the strain focuses on a smaller zone, thus "freezing" in the hanging wall a part of the former trishear zone and related structures [*Allmendinger*, 1998]. The folds associated with F3 and F4 are narrower, so that we use this approach to reproduce their geometry and "freeze" part of the deformation during the fault propagation. The trishear angle is constrained by our model with a variability of 10°. The *P*/*S* ratio is one of the most important parameters of trishear modeling. It controls the degree of folding accommodated in the trishear zone. A *P*/*S* ratio of 0 (footwall fixed) or 1 (hanging wall fixed) forms open and gentle folds. On the opposite, if the *P*/*S* ratio is important (>2), the degree of folding decreases and we obtain a narrow zone of deformation close to the fault. Several natural examples have been modeled with *P*/*S* ratios ranging from 0 to 9 and most commonly between 2 and 3 [*Allmendinger*, 1998; *Gold et al*., 2006; *Cardozo and Aanonsen*, 2009; *Pei et al*., 2014]. In our model, the *P*/*S* ratio for faults F1 to F3 is below 2. For the last fault reaching the surface, F4, the

deformation is more localized on the fault. We thus use a larger *P/S* ratio with a value of 2.5–3.5 consistent with a narrower zone of deformation. It is difficult to quantify the real uncertainty on the *P/S* ratio; we estimate our *P/S* ratios reasonable as they are in the range of values proposed in the literature from the modeling of other natural examples.

Our kinematic model has been elaborated in a forward process, and best fit parameters were not obtained from inversions. To this respect, we acknowledge that our solution depicted in Figure 7 is not unique. However, this has no impact on our first-order results on the main three characteristics of the WAFTB: (1) an unambiguous westward propagating fold-thrust belt over a décollement, (2) its associated finite shortening, and (3) its timing of deformation derived from our structural section (Figures 6 and 8). Our kinematic modeling is used here only to illustrate graphically a probable growth mechanism of the WAFTB and our inferences in terms of cumulative shortening (see hereafter, section 5.3).

5.2. Surface Processes and/or Structural Inheritance Control on the Kinematics of the West Andean Fold-and-Thrust Belt

The reconstruction also suggests that the faults forming the large west verging folds of the WAFTB become closely spaced and closer to the surface as we approach the western front. This may be explained by a change in deformation behavior, medium properties, or inherited structures. *Fillon et al*. [2013] proposed that the length of thrust sheets within fold-and-thrust belts increases with syntectonic sediment thicknesses. The average thrust-sheet length within the WAFTB is of 5–12 km for a syntectonic Farellones sediment thickness between 0 and 3.5 km. These values appear to be consistent with the compilation of data by *Fillon et al*. [2013] from eight fold-and-thrust belts around the world. Such reasoning also seems to hold for individual thrust sheets of the WAFTB. Indeed, the length of thrust sheets decreases westward along with the thickness of the Farellones formation. The fold wavelength decreases from 9–13 km between F0 and F1 to 3–9 km between F2-F3 and F3-F4, consistent with the decrease in the thickness of the Farellones formation from 3 to 4 km nearby the Cerro Quempo to less than 1 km on the eastern flank of the Cerro San Ramón. Syntectonic sedimentation of the Farellones formation may have therefore impacted the structural evolution of the WAFTB within our study area, in addition to the significant thickness of the sedimentary pile involved in the thrust belt.

The WAFTB is interpreted to root on a low-angle, eastward dipping décollement at—or close to—the base of the Andean basin within a possible Jurassic gypsum layer. Late Jurassic and/or Cretaceous gypsum ductile layers are well known for their determinant contribution to significant diapirism and décollement of the Mesozoic and Cenozoic cover above the basement of the Frontal Cordillera. These layers are observed in the thin series of the shallow Aconcagua fold-and-thrust belt, east of our study area [*Giambiagi*, 2003]. However, gypsum layers are also observed in the 9–10 km verticalized, thick Mesozoic series of the west vergent folds, in particular in the Valle del Yeso [*Thiele*, 1980; *Armijo et al*., 2010]. These exhumed, verticalized series have been used to infer the thickness of the Andean basin at depth, with the observed gypsum layer located at the base of the series suggesting a possible localization of the basal décollement in this layer. To the west, close to the Coastal Cordillera, no such layer has been found within the dominantly volcanic Mesozoic pile. This may suggest a disappearance of the gypsum layer somewhere in the middle of the Andean basin. However, we do not have a precise knowledge of the geometry of this gypsum layer. The presence or absence of a low basal friction décollement can have a major impact on the structural style of a thrust belt. It has been shown that gypsum provides a very low friction décollement and promotes the development of long thrust sheets [*Nieuwland et al*., 2000]. Changing from a gypsum décollement to a higher friction décollement results in the decrease of the length of the thrust sheets [*Nieuwland et al*., 2000, 2001]. The structural style and probable evolution of the WAFTB may therefore also illustrate the mechanical properties of the layers involved during faulting and folding, as inherited from sedimentation within the earlier Andean basins.

5.3. Shortening Rates Over Different Time and Space Scales and Implications for Seismic Hazard in Santiago

Our kinematic reconstruction allows for deriving cumulative shortening over time. Long-term average shortening rate across the WAFTB is found to be between 0.3 and 0.5 mm/yr over the last 25 Myr (Figure 8), a value consistent with the minimum shortening rate of 0.4 mm/yr proposed by *Armijo et al*. [2010]. The range of

possible shortening rates is derived from the range of cumulative shortening and timing of deformation resulting from our step-by-step interpretation. This interpretation is associated with large uncertainties on shortening and timing (see Figure 8). Speculating at a more detailed level, however, our analysis may suggest an initial higher shortening rate of ~1.7 mm/yr with a possible decrease of shortening rate at ~18–22 Ma to 0.1–0.5 mm/yr (Figure 8). This trend is derived only from the initial step of deformation in our kinematic modeling procedure (Figure 7), which may appear as a very weak constraint. However, the possible higher initial rate is inferred from the occurrence of a clear erosion surface and unconformity between the Abanico and Farellones formations over the anticline associated to F2 and within the western limb of the anticline associated to F1. This unconformity places a definite geometric constraint on the amount of deformation needed between the end of deposition of the Abanico formation and initiation of that of the Farellones formation. If the early cumulative shortening on F1 and F2 from our geological observations is correct, then the initially higher shortening rate could be an artifact caused by underestimating the age of the top deposits associated with the Abanico formation. Keeping the initial cumulative shortening on F1 and F2 constant and considering a shortening rate of 0.1–0.5 mm/yr would suggest that deposition of the Abanico formation stopped by 40–45 Ma, which is inconsistent with published ages [*Charrier et al*., 2002]. Consistency with present age constraints requires the occurrence of the shortening rate decrease at ~18–22 Ma, as suggested by our results in Figure 8. Furthermore, the suggested shortening rate decrease across the WAFTB at ~18–22 Ma implies transfer of slip from the WAFTB to other fault systems located eastward across the Andes, with slip rates of ~0.9–1.2 mm/yr or more. One likely system may be the Aconcagua fold-and-thrust belt starting by this time [*Giambiagi et al*., 2001; *Armijo et al*., 2010]. This is presently being further investigated.

Our 0.1 to 0.5 mm/yr average shortening rate across the WAFTB represents a fraction of the total crustal shortening and thickening required by Andean mountain building and is 2 orders of magnitude less than the 6–7 cm/yr of Nazca-South America total plate convergence rate at this latitude [e.g., *Altamimi et al*., 2007], which is absorbed mainly by seismic slip during megathrust earthquakes at the subduction zone.

Armijo et al. [2010] have discovered and mapped a 15 km long segment with a conspicuous piedmont scarp at the outskirts of Santiago, defining clearly the trace of the San Ramón fault, which is the most frontal thrust ramp of the WAFTB. By combining high-resolution imagery, digital topography, and dating of Pleistocene sediments of the piedmont (Ar/Ar ages from pumice rhyolitic pyroclastic deposits and optically stimulated luminescence), these authors suggest a slip rate of ~0.3 mm/yr for the San Ramón fault over the last 16 Ma. *Vargas et al*. [2014] dug a couple of trenches across the piedmont scarp documenting occurrence of surface rupture during two M_w ~7.5 earthquakes over the past 17–19 kyr, each one with a thrust slip of ~5 m on a fault reaching the surface with ~20° eastward dip. From these results, a near-surface slip rate on the San Ramón fault of nearly ~0.5 mm/yr (or ~0.45 mm/yr horizontal shortening rate) for the past ~20 kyr can be deduced and compares well with our shortening rates deduced over the past ~25 Myr across the whole WAFTB (Figure 8). Therefore, we find that our long-term results are consistent with the most recent seismic activity on the San Ramón fault, but that recent activity tends to favor the higher long-term shortening rate value of ~0.5 mm/yr. Because the seismic cycle of the San Ramón fault may not be time or slip predictable, the two most recent paleo-earthquakes may not be representative of the overall seismic behavior of the San Ramón fault. Also, the ~5 m surface coseismic slip measured for each paleo-earthquake may not be representative of the average coseismic slip occurring on the whole fault plane during these two events. In any case, consistency of the paleoseismic observations on the San Ramón fault with our results on the WAFTB emphasizes the idea that the San Ramón fault is most probably the only presently active fault across the section of the WAFTB in front of Santiago and indicates that most—if not all—the deformation across this fold-and-thrust belt is to be released seismically during earthquakes breaking the San Ramón fault up to the surface.

6. Conclusions

By combining field observations and geological maps together with satellite imagery and digital elevation models, we performed a precise 3-D geological map of the WAFTB east of Santiago (central Chile). We then projected our data across the region to build a geological cross section. Following previous authors [*Armijo et al*., 2010], we interpreted folding at the surface in terms of five faults rooting at depth onto one décollement. The timing of deformation of these faults was precisely constrained from the angular

unconformity between Farellones and Abanico formations derived from our 3-D mapping and subsequent projection. From there, we proposed that deformation of the West Andean fold-and-thrust belt initiated by ~25 Ma and that it evolved as a westward propagating fault system. To further explore and test the kinematics derived from our geological observations, we built a forward kinematic model using the trishear formalism. We incrementally rebuilt the kinematics of the WAFTB and quantified the evolution of cumulative shortening over time. Our results suggest an average shortening rate across the WAFTB of 0.1–0.5 mm/yr since ~18–22 Ma, with a possible decrease at ~25 Ma from an initially higher value of ~1.7 mm/yr. This deformation rate appears consistent with recent paleo-seismological findings on the San Ramón fault, at the forefront of the WAFTB. This suggests that the San Ramón fault is most probably the presently only active fault of the WAFTB and that most—if not all—the deformation across the fold-and-thrust belt is to be released seismically.

Acknowledgments

Work supported by a PhD grant attributed to M. Riesner by the Ministry of Higher Education and Research and funded by ANR project MegaChile (grant ANR-12-BS06-0004-02) and LABEX UnivEarthS project (Sorbonne Paris Cité, Work Package 1). We thank Daniel Carrizo and AMTC (Universidad de Chile) for organizing and funding the helicopter fly over the WAFTB. The kinematic modeling was made using FoldFault FORWARD version 6, freely available from http://www.geo.cornell.edu/geology/faculty/RWA/programs/faultfoldforward.html [*Allmendinger*, 1998]. This manuscript benefitted from the constructive reviews of R.W. Allmendinger, V.A. Ramos, and of an anonymous reviewer. This is IPGP contribution 3818.

References

Aguirre, L., D. Robinson, R. E. Bevins, D. Morata, M. Vergara, E. Fonseca, and J. Carrasco (2000), A low-grade metamorphic model for the Miocene volcanic sequences in the Andes of central Chile, *N. Z. J. Geol. Geophys.*, *43*(1), 83–93, doi:10.1080/00288306.2000.9514871.

Allmendinger, R. W. (1998), Inverse and forward numerical modeling of trishear fault-propagation folds, *Tectonics*, *17*, 640–656, doi:10.1029/98TC01907.

Allmendinger, R. W., and P. A. Judge (2014), The Argentine Precordillera: A foreland thrust belt proximal to the subducted plate, *Geosphere*, *10*(6), doi:10.1130/ges01062.1.

Allmendinger, R. W., and J. H. Shaw (2000), Estimation of fault propagation distance from fold shape: Implications for earthquake hazard assessment, *Geology*, *28*(12), 1099–1102.

Altamimi, Z., X. Collilieux, J. Legrand, B. Garayt, and C. Boucher (2007), ITRF2005: A new release of the International Terrestrial Reference Frame based on time series of station positions and Earth Orientation Parameters, *J. Geophys. Res.*, *112*, B09401, doi:10.1029/2007JB004949.

Armijo, R., R. Rauld, R. Thiele, G. Vargas, J. Campos, R. Lacassin, and E. Kausel (2010), The West Andean Thrust, the San Ramón fault, and the seismic hazard for Santiago, Chile, *Tectonics*, *29*, TC2007, doi:10.1029/2008TC002427.

Armijo, R., R. Lacassin, A. Coudurier-Curveur, and D. Carrizo (2015), Coupled tectonic evolution of Andean orogeny and global climate, *Earth Sci. Rev.*, doi:10.1016/j.earscirev.2015.01.005.

Beccar, I., M. Vergara, and F. Munizaga (1986), Edades K/Ar de la formación Farellones, en el cordón del cerro La Parva, Cordillera de Los Andes de Santiago, *Rev. Geol. Chile*, *28–29*, 109–113.

Borde, J. (1966), Les Andes de Santiago et leur avant- pays. Etude de geómorphologie, Doctorate thesis, 599 pp., Univ. Bordeaux 1, Talence, France.

Cardozo, N., and S. Aanonsen (2009), Optimized trishear inverse modeling, *J. Struct. Geol.*, *31*, 546–560.

Charrier, R., O. Baeza, S. Elgueta, J. J. Flynn, P. Gans, S. M. Kay, N. Muñoz, A. R. Wyss, and E. Zurita (2002), Evidence for Cenozoic extensional basin development and tectonic inversion south of the flat-slab segment, southern central Andes, Chile (33°–36°S.L.), *J. South Am. Earth Sci.*, *15*, 117–139, doi:10.1016/S0895-9811(02)00009-3.

Charrier, R., M. Bustamante, D. Comte, S. Elgueta, J. J. Flynn, N. Iturra, N. Muñoz, M. Pardo, R. Thiele, and A. R. Wyss (2005), The Abanico extensional basin: Regional extension, chronology of tectonic inversion and relation to shallow seismic activity and Andean uplift, Neues Jahrb, *Geol. Palaeontol. Abh.*, *236*, 43–77.

Charrier, R., L. Pinto, and M. P. Rodríguez (2007), Tectonostatigraphic evolution of the Andean orogen in Chile, in *The Geology of Chile*, edited by T. Moreno and W. Gibbons, pp. 21–114, Geol. Soc., London.

Cornejo, P., and G. Mahood (1997), Seeing past the effects of re-equilibration to reconstruct magmatic gradients in plutons: La Gloria Pluton, central Chilean Andes, *Contrib. Miner. Petrol.*, *127*, 159–175.

Cristallini, E. O., and R. W. Allmendinger (2002), Backlimb trishear: A kinematic model for curved folds developed over angular fault bends, *J. Struct. Geol.*, *24*, 289–295.

Deckart, K., A. H. Clark, C. Aguilar, R. Vargas, A. Bertens, J. K. Mortensen, and M. Fanning (2005), Magmatic and hydrothermal chronology of the giant Río Blanco porphyry copper deposit, central Chile: Implications of an integrated U-Pb and $^{40}Ar/^{39}Ar$ database, *Econ. Geol.*, *100*, 905–934, doi:10.2113/100.5.905.

Deckart, K., E. Godoy, A. Bertens, D. Jerez, and A. Saeed (2010), Barren Miocene granitoids in the central Andean metallogenic belt, Chile: Geochemistry and Nd-Hf and U-Pb isotope systematics, *Andean Geol.*, *37*(1), 1–31.

Dewey, J. F., and J. M. Bird (1970), Mountain belts and the new global tectonics, *J. Geophys. Res.*, *75*, 2625–2627, doi:10.1029/JB075i014p02625.

Erslev, E. A. (1991), Trishear fault-propagation folding, *Geology*, *19*, 617–620, doi:10.1130/0091-7613(1991)019<0617:TFPF>2.3.CO;2.

Farías, M., D. Comte, R. Charrier, J. Martinod, and C. David (2010), Crustal-scale structural architecture in central Chile based on seismicity and surface geology: Implications for Andean mountain building, *Tectonics*, *29*, TC3006, doi:10.1029/2009TC002480.

Fillon, C., R. Huismans, and P. van der Beek (2013), Syntectonic sedimentation effects on the growth of fold-and-thrust belts, *Geology*, *41*, 83–86.

Fock, A. (2005), Cronología y tectónica de la exhumación en el Neógeno de los Andes de Chile central entre los 33° y los 34° S, Tésis para optar al grado de Magíster en Ciencias, Mención Geología, Memoria para optar al título de Geólogo, thesis, 179 pp., Dep. de Geol., Univ. de Chile, Santiago.

Fosdick, J. C., B. Carrapa, and G. Ortiz (2015), Faulting and erosion in the Argentine Precordillera during changes in subduction regime: Reconciling bedrock cooling and detrital records, *Earth Planet. Sci. Lett.*, *432*, 73–83.

Gana, P., and R. Wall (1997), Evidencias geocronólogicas Ar/Ar y K/Ar de un hiatus Cretácico Superior-Eoceno en Chile central (33°–33°30′S), *Rev. Geol. Chile*, *24*(2), 145–163.

Gana, P., D. Sellés, and R. Wall (1999), Mapa geológico area Tiltil-Santiago, región metropolitana, Mapas Geol.11, scale 1:100,000, Serv. Nac. de Geol. y Miner., Santiago.

García, V. H., and A. Casa (2014), Quaternary tectonics and seismic potential of the Andean retrowedge at 338–348°S, in *Geodynamic Processes in the Andes of Central Chile and Argentina*, edited by S. A. Sepulveda, et al., *Geol. Soc. London Spec. Publ.*, 399, doi:10.1144/SP399.11

Giambiagi, L., J. Mescua, F. Bechis, A. Martínez, and A. Folguera (2011), Pre-Andean deformation of the Precordillera southern sector, southern central Andes, *Geosphere*, *7*, 1–21.
Giambiagi, L., et al. (2014), Reactivation of Paleozoic structures during Cenozoic deformation in the Cordón del Plata and southern Precordillera ranges (Mendoza, Argentina), *J. Iber. Geol.*, *40*, 309–320.
Giambiagi, L. B. (2003), Deformación cenozoica de la faja plegada y corrida del Aconcagua y Cordillera Frontal, entre los 33°30′ y 33°45′S, *Asoc. Geol. Argent. Rev.*, *58*, 85–96.
Giambiagi, L. B., M. Tunik, and M. Ghiglione (2001), Cenozoic tectonic evolution of the Alto Tunuyán foreland basin above the transition zone between the flat and normal subduction segment (33°30′–34°S), western Argentina, *J. South Am. Earth Sci.*, *14*, 707–724, doi:10.1016/S0895-9811(01)00059-1.
Giambiagi, L. B., V. A. Ramos, E. Godoy, P. P. Alvarez, and S. Orts (2003), Cenozoic deformation and tectonic style of the Andes, between 33° and 34° south latitude, *Tectonics*, *22*(4), 1041, doi:10.1029/2001TC001354.
Gold, R. D., E. Cowgill, X. F. Wang, and X. H. Chen (2006), Application of trishear fault-propagation folding to active reverse faults: Examples from the Dalong Fault, Gansu Province, NW China, *J. Struct. Geol.*, *28*, 200–219.
Hardy, S., and M. Ford (1997), Numerical modeling of trishear fault-propagation folding and associated growth strata, *Tectonics*, *16*, 841–854, doi:10.1029/97TC01171.
James, D. E. (1971), Plate tectonic model for the evolution of the central Andes, *Geol. Soc. Am. Bull.*, *82*, 3325–3346, doi:10.1130/0016-7606(1971)82[3325:PTMFTE]2.0.CO;2.
Kurtz, A., S. Kay, R. Charrier, and E. Farrar (1997), Geochronology of Miocene plutons and exhumation history of the El Teniente region, central Chile (34–35°S, *Rev. Geol. Chile*, *24*, 75–90.
Mpodozis, C., and V. A. Ramos (1989), The Andes of Chile and Argentina, in *Geology of the Andes and Its Relation to Hydrocarbon and Mineral Resources*, *Earth Sci. Ser.*, vol. 11, edited by G. E. Ericksen, M. T. Cañas Pinochet, and J. A. Reinemund, pp. 59–90, Circum Pac. Counc. for Energy and Miner. Resour., Houston, Tex.
Nieuwland, D. A., J. H. Leutscher, and J. Gast (2000), Wedge equilibrium in fold-and-thrust belts: Prediction of out-of-sequence thrusting based on sandbox experiments and natural examples, *Geol. Mijnbouw/Neth. J. Geosci.*, *79*(1), 81–91.
Nieuwland, D. A., B. C. Oudmayer, and U. Valbona (2001), The tectonic development of Albania: Explanation and prediction of structural styles, *Mar. Pet. Geol.*, *18*, 161–177.
Nyström, J. O., M. Vergara, D. Morata, and B. Levi (2003), Tertiary volcanism during extension in the Andean foothills of central Chile (33°15′–33°45′S), *Geol. Soc. Am. Bull.*, *115*, 1523–1537, doi:10.1130/B25099.1.
Pei, Y., D. A. Paton, and R. J. Knipe (2014), Defining a 3-dimensional trishear parameter space to understand the temporal evolution of fault propagation folds, *J. Struct. Geol.*, *6*, 284–297.
Pérez, A., J. A. Ruiz, G. Vargas, R. Rauld, S. Rebolledo, and J. Campos (2013), Improving seismotectonics and seismic hazard assessment along the San Ramón fault at the eastern border of Santiago City, Chile, *Nat. Hazards*, *71*, 243–274, doi:10.1007/s11069-013-0908-3.
Ramos, V. A., M. L. Cegarra, and E. Cristallini (1996), Cenozoic tectonics of the High Andes of west/central Argentina (30°–36°S latitude), *Tectonophysics*, *259*, 185–200, doi:10.1016/0040-1951(95)00064-X.
Ramos, V. A., T. Zapata, E. Cristallini, and A. Introcaso (2004), The Andean thrust system—Latitudinal variations in structural styles and orogenic shortening, in *Thrust Tectonics and Hydrocarbon Systems*, edited by K. R. McClay, *AAPG Mem.*, *82*, 30–50.
Rauld, R. A. (2011), Deformación cortical y peligro sismico asociado a la falla San Ramón en el Frente Cordillerano de Santiago, Chile central (33°S). Tésis para optar al grado de Doctor en Ciencias, Mención Geología, 443 pp., Dep. de Geol., Univ. de Chile, Santiago.
Robinson, D., R. Bevins, L. Aguirre, and M. Vergara (2004), A reappraisal of episodic burial metamorphism in the Andes of central Chile, *Contrib. Mineral. Petrol.*, *146*, 513–528, doi:10.1007/s00410-003-0516-4.
Sellés, D., and P. Gana (2001), Geología del Area Talagante–San Francisco de Mostazal, Regiones Metropolitana de Santiago y del Libertador General Bernardo O'Higgins, Carta Geológica de Chile, Ser. Geol. Básica 74, scale 1:100,000, 30 pp., Serv. Nac. de Geol. y Miner., Santiago.
Thiele, R. (1980), Geología de la hoja Santiago, Región Metropolitana, Carta Geológica de Chile, scale 1:250,000, pp. 51, Inst. de Invest. Geol., Santiago.
Tricart, J., A. R. Hirsch, and J. C. Griesbach (1965), Geomorphologie et eaux souterraines dans le basin de Santiago du Chili, *Bull. Fac. Lett. Strasbourg*, *7*, 605–673.
Vargas, G., Y. Klinger, T. K. Rockwell, S. L. Forman, S. Rebolledo, S. Baize, R. Lacassin, and R. Armijo (2014), Probing large intraplate earthquakes at the west flank of the Andes, *Geology*, doi:10.1130/G35741.1.
Vergara, M., and R. Drake (1979), Eventos magmaticos-plutonicos en Los Andes de Chile Central. In : II Congreso Geologico Chileno. 2., Arica, 6–11 Agosto, F19–F30.
Vergara, M., R. Charrier, F. Munizaga, S. Rivano, P. Sepulveda, R. Thiele, and R. Drake (1988), Miocene volcanism in the central Chilean Andes (31°30′S–34°35′S), *J. South Am. Earth Sci.*, *1*, 199–209, doi:10.1016/0895-9811(88)90038-7.
Vergara, M., L. López-Escobar, J. L. Palma, R. Hickey-Vargas, and C. Roeschmann (2004), Late Tertiary volcanic episodes in the area of the city of Santiago de Chile: New geochronological and geochemical data, *J. South Am. Earth Sci.*, *17*, 227–238, doi:10.1016/j.jsames.2004.06.003.
Vicente, J. C. (2005), Dynamic paleogeography of the Jurassic Andean Basin: Pattern of transgression and localisation of main straits through the magmatic arc, *Asoc. Geol. Argent. Rev.*, *60*, 221–250.
Zehnder, A. T., and R. W. Allmendinger (2000), Velocity field for the trishear model, *J. Struct. Geol.*, *22*, 1009–1014.